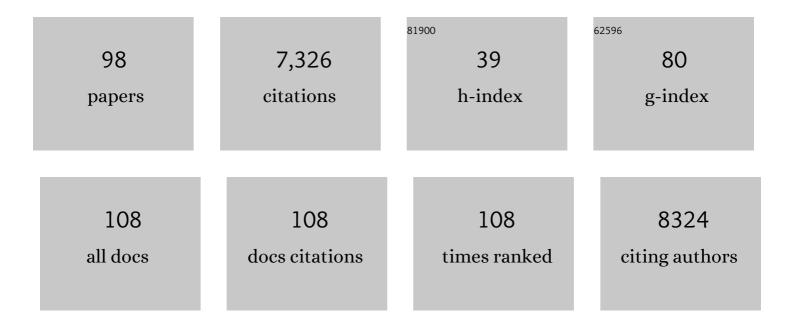
## Kamil Uludag

List of Publications by Year in descending order

Source: https://exaly.com/author-pdf/3742729/publications.pdf Version: 2024-02-01



KAMII HLUDAC

#	Article	IF	CITATIONS
1	Modeling the hemodynamic response to brain activation. Neurolmage, 2004, 23, S220-S233.	4.2	1,023
2	Simultaneous PET-MRI: a new approach for functional and morphological imaging. Nature Medicine, 2008, 14, 459-465.	30.7	1,008
3	An integrative model for neuronal activity-induced signal changes for gradient and spin echo functional imaging. NeuroImage, 2009, 48, 150-165.	4.2	381
4	Coupling of cerebral blood flow and oxygen consumption during physiological activation and deactivation measured with fMRI. NeuroImage, 2004, 23, 148-155.	4.2	230
5	Locus coeruleus imaging as a biomarker for noradrenergic dysfunction in neurodegenerative diseases. Brain, 2019, 142, 2558-2571.	7.6	219
6	Towards a standard analysis for functional near-infrared imaging. Neurolmage, 2004, 21, 283-290.	4.2	213
7	General overview on the merits of multimodal neuroimaging data fusion. Neurolmage, 2014, 102, 3-10.	4.2	179
8	The Influence of Moderate Hypercapnia on Neural Activity in the Anesthetized Nonhuman Primate. Cerebral Cortex, 2008, 18, 2666-2673.	2.9	144
9	Linking brain vascular physiology to hemodynamic response in ultra-high field MRI. NeuroImage, 2018, 168, 279-295.	4.2	137
10	Habituation of the Visually Evoked Potential and Its Vascular Response: Implications for Neurovascular Coupling in the Healthy Adult. NeuroImage, 2002, 17, 1-18.	4.2	126
11	Cross talk in the Lambert-Beer calculation for near-infrared wavelengths estimated by Monte Carlo simulations. Journal of Biomedical Optics, 2002, 7, 51.	2.6	119
12	Investigating the post-stimulus undershoot of the BOLD signal—a simultaneous fMRI and fNIRS study. NeuroImage, 2006, 30, 349-358.	4.2	115
13	Caffeine alters the temporal dynamics of the visual BOLD response. NeuroImage, 2004, 23, 1402-1413.	4.2	113
14	Physiologically informed dynamic causal modeling of fMRI data. NeuroImage, 2015, 122, 355-372.	4.2	109
15	Subthalamic Nucleus Deep Brain Stimulation: Basic Concepts and Novel Perspectives. ENeuro, 2017, 4, ENEURO.0140-17.2017.	1.9	106
16	Individualized parcellation of the subthalamic nucleus in patients with Parkinson's disease with 7T MRI. NeuroImage, 2018, 168, 403-411.	4.2	106
17	High-resolution in vivo imaging of human locus coeruleus by magnetization transfer MRI at 3T and 7T. NeuroImage, 2018, 168, 427-436.	4.2	104
18	Separability and cross talk: optimizing dual wavelength combinations for near-infrared spectroscopy of the adult head. NeuroImage, 2004, 22, 583-589.	4.2	101

KAMIL ULUDAG

#	Article	IF	CITATIONS
19	The effect of spatial resolution on decoding accuracy in fMRI multivariate pattern analysis. NeuroImage, 2016, 132, 32-42.	4.2	101
20	Techniques for blood volume fMRI with VASO: From low-resolution mapping towards sub-millimeter layer-dependent applications. NeuroImage, 2018, 164, 131-143.	4.2	101
21	Determining Excitatory and Inhibitory Neuronal Activity from Multimodal fMRI Data Using a Generative Hemodynamic Model. Frontiers in Neuroscience, 2017, 11, 616.	2.8	98
22	Non-BOLD contrast for laminar fMRI in humans: CBF, CBV, and CMRO2. NeuroImage, 2019, 197, 742-760.	4.2	96
23	The impact of ultra-high field MRI on cognitive and computational neuroimaging. NeuroImage, 2018, 168, 366-382.	4.2	93
24	Noninvasive monitoring of cerebral blood flow by a dye bolus method: Separation of brain from skin and skull signals. Journal of Biomedical Optics, 2002, 7, 464.	2.6	88
25	Aerobic Exercise Training Improves Cerebral Blood Flow and Executive Function: A Randomized, Controlled Cross-Over Trial in Sedentary Older Men. Frontiers in Aging Neuroscience, 2019, 11, 333.	3.4	86
26	A dynamical model of the laminar BOLD response. NeuroImage, 2020, 204, 116209.	4.2	78
27	Functional localization in the human brain: Gradientâ€echo, spinâ€echo, and arterial spin″abeling fMRI compared with neuronavigated TMS. Human Brain Mapping, 2011, 32, 341-357.	3.6	74
28	Comparison of pulsed arterial spin labeling encoding schemes and absolute perfusion quantification. Magnetic Resonance Imaging, 2009, 27, 1039-1045.	1.8	72
29	Impact of acquisition and analysis strategies on cortical depth-dependent fMRI. NeuroImage, 2018, 168, 332-344.	4.2	71
30	Layer-dependent functional connectivity methods. Progress in Neurobiology, 2021, 207, 101835.	5.7	67
31	Cortical depth profiles of luminance contrast responses in human V1 and V2 using 7 T fMRI. Human Brain Mapping, 2018, 39, 2812-2827.	3.6	59
32	Frontiers of brain mapping using MRI. Journal of Magnetic Resonance Imaging, 2006, 23, 945-957.	3.4	58
33	Predictors of Response to Treadmill Exercise in Stroke Survivors. Neurorehabilitation and Neural Repair, 2010, 24, 567-574.	2.9	57
34	Convergence of human brain mapping tools: Neuronavigated TMS Parameters and fMRI activity in the hand motor area. Human Brain Mapping, 2012, 33, 1107-1123.	3.6	56
35	Dynamics and nonlinearities of the BOLD response at very short stimulus durations. Magnetic Resonance Imaging, 2008, 26, 853-862.	1.8	54
36	Resolving laminar activation in human V1 using ultra-high spatial resolution fMRI at 7T. Scientific Reports, 2018, 8, 17063.	3.3	53

KAMIL ULUDAG

#	Article	IF	CITATIONS
37	Spatial representations of temporal and spectral sound cues in human auditory cortex. Cortex, 2013, 49, 2822-2833.	2.4	50
38	Reproducibility and Reliability of Quantitative and Weighted T1 and T2â^— Mapping for Myelin-Based Cortical Parcellation at 7 Tesla. Frontiers in Neuroanatomy, 2016, 10, 112.	1.7	49
39	Ultra-high field magnetic resonance imaging of the basal ganglia and related structures. Frontiers in Human Neuroscience, 2014, 8, 876.	2.0	47
40	Transient and sustained BOLD responses to sustained visual stimulation. Magnetic Resonance Imaging, 2008, 26, 863-869.	1.8	46
41	Direct measurement of oxygen extraction with fMRI using 6% CO2 inhalation. Magnetic Resonance Imaging, 2008, 26, 961-967.	1.8	45
42	Ultra-high resolution blood volume fMRI and BOLD fMRI in humans at 9.4†T: Capabilities and challenges. NeuroImage, 2018, 178, 769-779.	4.2	44
43	Neurovascular coupling analyzed non-invasively in the human brain. NeuroReport, 2004, 15, 63-66.	1.2	43
44	Dynamic behavior of the locus coeruleus during arousal-related memory processing in a multi-modal 7T fMRI paradigm. ELife, 2020, 9, .	6.0	43
45	Quantifying the Link between Anatomical Connectivity, Gray Matter Volume and Regional Cerebral Blood Flow: An Integrative MRI Study. PLoS ONE, 2011, 6, e14801.	2.5	42
46	Ultra-High Field MRI Post Mortem Structural Connectivity of the Human Subthalamic Nucleus, Substantia Nigra, and Globus Pallidus. Frontiers in Neuroanatomy, 2016, 10, 66.	1.7	42
47	Unraveling the contributions to the neuromelanin-MRI contrast. Brain Structure and Function, 2020, 225, 2757-2774.	2.3	41
48	Cytochrome-c-oxidase redox changes during visual stimulation measured by near-infrared spectroscopy cannot be explained by a mere cross talk artefact. NeuroImage, 2004, 22, 109-119.	4.2	39
49	Pulsatility of Lenticulostriate Arteries Assessed by 7 Tesla Flow MRI—Measurement, Reproducibility, and Applicability to Aging Effect. Frontiers in Physiology, 2017, 8, 961.	2.8	39
50	The impact of correction on <scp>MP2RAGE</scp> cortical <scp>T</scp> <sub>1</sub> and apparent cortical thickness at 7 <scp>T</scp> . Human Brain Mapping, 2018, 39, 2412-2425.	3.6	38
51	Neural activity-induced modulation of BOLD poststimulus undershoot independent of the positive signal. Magnetic Resonance Imaging, 2009, 27, 1030-1038.	1.8	37
52	Interleaved TMS/CASL: Comparison of different rTMS protocols. NeuroImage, 2010, 49, 612-620.	4.2	37
53	Dopplersonographic measurement of global cerebral circulation time using echo contrast-enhanced ultrasound in normal individuals and patients with arteriovenous malformations. Ultrasound in Medicine and Biology, 2002, 28, 453-458.	1.5	35
54	Relevance of depth resolution for cerebral blood flow monitoring by near-infrared spectroscopic bolus tracking during cardiopulmonary bypass. Journal of Thoracic and Cardiovascular Surgery, 2006, 132, 1172-1178.	0.8	34

Kamil Uludag

#	Article	IF	CITATIONS
55	On the feasibility of concurrent human TMS-EEG-fMRI measurements. Journal of Neurophysiology, 2013, 109, 1214-1227.	1.8	34
56	Comparison of 3 T and 7 T ASL techniques for concurrent functional perfusion and BOLD studies. NeuroImage, 2017, 156, 363-376.	4.2	34
57	Neuroimaging with ultra-high field MRI: Present and future. NeuroImage, 2018, 168, 1-6.	4.2	33
58	To dip or not to dip: Reconciling optical imaging and fMRI data. Proceedings of the National Academy of Sciences of the United States of America, 2010, 107, E23; author reply E24.	7.1	32
59	Distortion-matched T1 maps and unbiased T1-weighted images as anatomical reference for high-resolution fMRI. NeuroImage, 2018, 176, 41-55.	4.2	32
60	Decreases in ADC observed in tissue areas during activation in the cat visual cortex at 9.4 T using high diffusion sensitization. Magnetic Resonance Imaging, 2008, 26, 889-896.	1.8	29
61	Sub-millimetre resolution laminar fMRI using Arterial Spin Labelling in humans at 7 T. PLoS ONE, 2021, 16, e0250504.	2.5	27
62	Differential effects of intranasal insulin and caffeine on cerebral blood flow. Human Brain Mapping, 2012, 33, 280-287.	3.6	26
63	On the importance of modeling fMRI transients when estimating effective connectivity: A dynamic causal modeling study using ASL data. NeuroImage, 2017, 155, 217-233.	4.2	24
64	Optimization of simultaneous multislice EPI for concurrent functional perfusion and BOLD signal measurements at 7T. Magnetic Resonance in Medicine, 2017, 78, 121-129.	3.0	24
65	Relationship of the BOLD Signal with VEP for Ultrashort Duration Visual Stimuli (0.1 to 5 ms) in Humans. Journal of Cerebral Blood Flow and Metabolism, 2010, 30, 449-458.	4.3	23
66	Volumetric imaging with homogenised excitation and static field at 9.4 T. Magnetic Resonance Materials in Physics, Biology, and Medicine, 2016, 29, 333-345.	2.0	23
67	Echo-time dependence of the BOLD response transients – A window into brain functional physiology. Neurolmage, 2017, 159, 355-370.	4.2	23
68	Functional cerebral blood volume mapping with simultaneous multi-slice acquisition. NeuroImage, 2016, 125, 1159-1168.	4.2	22
69	Direct visualization and characterization of the human zona incerta and surrounding structures. Human Brain Mapping, 2020, 41, 4500-4517.	3.6	21
70	On the numerically predicted spatial BOLD fMRI specificity for spin echo sequences. Magnetic Resonance Imaging, 2011, 29, 1195-1204.	1.8	20
71	Retinotopic maps and hemodynamic delays in the human visual cortex measured using arterial spin labeling. Neurolmage, 2012, 59, 4044-4054.	4.2	20
72	fMRI Adaptation between Action Observation and Action Execution Reveals Cortical Areas with Mirror Neuron Properties in Human BA 44/45. Frontiers in Human Neuroscience, 2016, 10, 78.	2.0	18

KAMIL ULUDAG

#	Article	IF	CITATIONS
73	European Ultrahighâ€Field Imaging Network for Neurodegenerative Diseases (EUFIND). Alzheimer's and Dementia: Diagnosis, Assessment and Disease Monitoring, 2019, 11, 538-549.	2.4	17
74	Effects of MP2RAGE B1+ sensitivity on inter-site T1 reproducibility and hippocampal morphometry at 7T. NeuroImage, 2021, 224, 117373.	4.2	17
75	Perfusion MRI using endogenous deoxyhemoglobin as a contrast agent: Preliminary data. Magnetic Resonance in Medicine, 2021, 86, 3012-3021.	3.0	17
76	Tonotopic maps in human auditory cortex using arterial spin labeling. Human Brain Mapping, 2017, 38, 1140-1154.	3.6	16
77	Anatomic & metabolic brain markers of the m.3243A>G mutation: A multi-parametric 7T MRI study. NeuroImage: Clinical, 2018, 18, 231-244.	2.7	15
78	Affected functional networks associated with sentence production in classic galactosemia. Brain Research, 2015, 1616, 166-176.	2.2	14
79	Letter to the editor. Magnetic Resonance in Medicine, 2004, 51, 1088-1089.	3.0	12
80	Improvement of sensitivity and specificity for laminar BOLD fMRI with double spin-echo EPI in humans at 7 T. NeuroImage, 2021, 241, 118435.	4.2	11
81	Determining laminar neuronal activity from BOLD fMRI using a generative model. Progress in Neurobiology, 2021, 207, 102055.	5.7	10
82	Regional effects of magnetization dispersion on quantitative perfusion imaging for pulsed and continuous arterial spin labeling. Magnetic Resonance in Medicine, 2013, 69, 524-530.	3.0	9
83	fMRI: From Nuclear Spins to Brain Functions. Biological Magnetic Resonance, 2015, , .	0.4	9
84	Latin American Brain Mapping Network (LABMAN). NeuroImage, 2009, 47, 312-313.	4.2	7
85	Quantitative and simultaneous measurement of oxygen consumption rates in rat brain and skeletal muscle using <sup>17</sup> 0 MRS imaging at 16.4T. Magnetic Resonance in Medicine, 2021, 85, 2232-2246.	3.0	7
86	Feedback contribution to surface motion perception in the human early visual cortex. ELife, 2020, 9, .	6.0	7
87	Network-based statistics for a community driven transparent publication process. Frontiers in Computational Neuroscience, 2012, 6, 11.	2.1	6
88	170 relaxation times in the rat brain at 16.4 tesla. Magnetic Resonance in Medicine, 2016, 75, 1886-1893.	3.0	6
89	Magnetic Field Distribution and Signal Decay in Functional MRI in Very High Fields (up to 9.4 T) Using Monte Carlo Diffusion Modeling. International Journal of Biomedical Imaging, 2007, 2007, 1-7.	3.9	5
90	Physiology and Physics of the fMRI Signal. Biological Magnetic Resonance, 2015, , 163-213.	0.4	5

Kamil Uludag

#	Article	IF	CITATIONS
91	Examples of sub-millimeter, 7T, T1-weighted EPI datasets acquired with the T123DEPI sequence. Data in Brief, 2018, 20, 415-418.	1.0	4
92	Combining fMRI with Other Modalities: Multimodal Neuroimaging. Biological Magnetic Resonance, 2015, , 739-768.	0.4	2
93	<title>Noninvasive cerebral blood flow monitoring by a dye bolus method:separation of extra- and intracerebral absorption changes by frequency-domain spectroscopy</title> ., 2001, , .		2
94	Neurodegenerative and functional signatures of the cerebellar cortex in m.3243A > G patients. Brain Communications, 2022, 4, fcac024.	3.3	2
95	Functional brain imaging by CW-NIRS coregistered by blood flow monitors. , 2003, , .		0
96	Investigating the physiology of brain activation with MRI. , 2004, , .		0
97	Functional MRI Dynamics. , 2015, , 81-87.		0
98	Optimization of simultaneous multislice EPI for concurrent functional perfusion and BOLD signal measurements at 7T. Magnetic Resonance in Medicine, 2017, 78, C1-C1.	3.0	0